Original Article

Baseline computed tomography imaging findings could assist in early diagnosis of visceral pleural invasion for newly discovered early subpleural non-small cell lung cancer: T1 or T2

Li Li[1,2,3#^], Qian Yang[2#^], Dehong Luo[2], Xiaoliang Wang[2^], Zhou Liu[2], Rong Huang[1,3^]

[1]Shantou University Medical College, Shantou, China; [2]Department of Radiology, National Cancer Center/National Clinical Research Center for Cancer/Cancer Hospital & Shenzhen Hospital, Chinese Academy of Medical Sciences and Peking Union Medical College, Shenzhen, China; [3]Department of Radiology, Peking University Shenzhen Hospital, Shenzhen, China

Contributions: (I) Conception and design: L Li, Z Liu, R Huang; (II) Administrative support: D Luo, R Huang; (III) Provision of study materials or patients: L Li, X Wang; (IV) Collection and assembly of data: L Li, Q Yang, X Wang; (V) Data analysis and interpretation: Q Yang, Z Liu; (VI) Manuscript writing: All authors; (VII) Final approval of manuscript: All authors.

[#]These authors contributed equally to this work.

Correspondence to: Rong Huang, MD. Shantou University Medical College, Shantou 515000, China; Department of Radiology, Peking University Shenzhen Hospital, 1120 Lotus Road, Futian District, Shenzhen 518034, China. Email: r.huang@pkuszh.com; Zhou Liu, MD, PhD. Department of Radiology, National Cancer Center/National Clinical Research Center for Cancer/Cancer Hospital & Shenzhen Hospital, Chinese Academy of Medical Sciences and Peking Union Medical College, 113 Baohe Avenue, Longgang District, Shenzhen 518116, China. Email: zhou_liu8891@yeah.net.

Background: Preoperative accurate visceral pleural infiltration (VPI) diagnosis for T1-size non-small cell lung cancer (NSCLC) is significant for clinical decision-making. The study aimed to explore the diagnostic efficacy of computed tomography (CT) imaging features and serum biomarkers in diagnosing VPI in newly discovered subpleural NSCLC ≤3 cm.

Methods: There were 447 patients with NSCLC ≤3 cm retrospectively enrolled and assigned to the VPI group (n=81) and the non-VPI group (n=366) based on elastic fiber staining results. The serum biomarkers and CT imaging features were obtained for each subject. Univariate and multivariate analyses were used to identify the independent predictors for VPI. Area under the receiver operating characteristic (ROC) curve (AUC) was used to evaluate the diagnostic performance of each independent predictor and combined predictors in predicting VPI, with performance compared using the DeLong test.

Results: For tumor biomarkers, the VPI group had a significantly higher percentage of cases with abnormal carcino-embryonic antigen (CEA) level, cytokeratin 19 fragment (CYFRA21-1) level, and pro-gastrin-releasing peptide (ProGRP) level than that of the non-VPI group (P<0.001, P=0.003, P=0.004). However, in multivariate analysis, only the lesion-pleura relationship patterns type Ia [odds ratio (OR) =20.689; 95% confidence interval (CI): 5.058–84.622; P<0.001], type Ib (OR =5.155; 95% CI: 1.178–22.552; P=0.03), type II (OR =7.154; 95% CI: 1.733–29.53; P=0.007) with type III as reference, solid lesion density (OR =9.954; 95% CI: 4.976–19.911; P<0.001) with part-solid density as reference were identified as the independent predictors for VPI. In predicting VPI, the combined model (AUC =0.885) significantly outperformed models based on lesion density (AUC =0.833) and lesion-pleura relationship patterns (AUC =0.655) (all P<0.001).

Conclusions: The CT predictors for VPI in patients with subpleural NSCLC (≤3 cm) were lesion density and lesion-pleura relationship patterns (pleural attachment and indentation), but not serum tumor biomarkers.

Keywords: Non-small cell lung cancer (NSCLC); visceral pleura invasion (VPI); serum biomarker; computed tomography (CT)

^ ORCID: Li Li, 0009-0002-1661-6304; Qian Yang, 0000-0002-1794-4409; Xiaoliang Wang, 0009-0001-2057-3733; Rong Huang, 0000-0003-0496-8628.

Submitted Feb 27, 2024. Accepted for publication Jul 19, 2024. Published online Sep 02, 2024.
doi: 10.21037/jtd-24-294
View this article at: https://dx.doi.org/10.21037/jtd-24-294

Introduction

Background

In 2020, lung cancer remained the most common cancer (2.2 million new cases and 11.4% of all new cancer cases) and the leading cause of death (1.8 million, 18%) worldwide (1). With the wide application of lung cancer screening for high-risk populations, a vast number of early non-small cell lung cancers (NSCLCs), especially those ≤3 cm in diameter, have been identified. Most of these newly identified NSCLCs have a close relationship with visceral pleura due to their predilection to locate in the sub-pleural region, which poses a challenge to clinicians and radiologists in clinical staging and treatment planning since visceral pleural invasion (VPI) has been proven as an unfavorable prognostic predictor directly affecting clinical staging (2,3). The presence of visceral pleura invasion would raise the clinical T stage from T1 to T2 for NSCLC (≤3 cm in diameter) in the ninth edition of staging system (4). Although it's still under debate regarding the right surgical approach for ≤3 cm staged IB NSCLC, since studies showed favorable (5) or comparable (2,6,7) outcomes for lobectomy over segmentectomy. However, most studies showed favorable outcomes for lobectomy over wedge resection (2,5). As a result, compared with T1-size VPI-free NSCLC, surgery with a larger extent might be a better choice for T1-size NSCLC with positive VPI (clinically staged T2) to have a better prognosis. Therefore, preoperative accurate diagnosis of VPI for T1-size NSCLC is of great significance for clinical decision-making.

Highlight box

Key findings

- Lung pure ground-glass nodule is a reliable negative predictor of the visceral pleural infiltration (VPI) for subpleural non-small cell lung cancer (NSCLC) (≤3 cm).
- Lesion density and lesion-pleura relationship patterns (pleural attachment and indentation) could assist in diagnosing VPI for newly discovered T1-size subpleural NSCLC.

What is known and what is new?

- Nodule density is the most important indicator for VPI.
- The longer the tumor-pleura contact length is, the more likely VPI is to occur.
- Tumor markers of lung cancer hold limited potential for predicting preoperativce VPI.

What is the implication, and what should change now?

- Nodule density and contact patterns between tumor and pleura should be taken into consideration when predicting VPI. However, tumor markers provides limited relevant information in the prediction of VPI.

Rationale and knowledge gap

In the clinical setting, chest high-resolution computed tomography (HRCT) is routinely used to perform on preoperative T stage (VPI prediction) of NSCLC (≤3 cm) for its capacity to depict detailed anatomical relationships between lesions and pleura. Previously, several common computed tomography (CT) imaging findings were identified across a few studies for VPI prediction, including direct pleural attachment (5,8-10), pleural indentation (11), pleural tags (9,12-15), pleural thickening (8,12). Some studies focused on a subset of T1-size NSCLC, such as adenocarcinoma (9,10,16-18), subsolid lesions (17,18), pure ground-glass nodule (GGN) (18), or lesions without direct contact to pleura (13,14). However, another study by Kim *et al.* showed that CT features should not be used to predict VPI due to a non-negligible high false-positive rate (as high as about 50%) (16). Besides CT imaging features, circulating tumor cell level was shown as an additional significant VPI predictor for invasive adenocarcinoma (≤3 cm), suggesting the potential of serum tumor-related markers in predicting VPI (9). However, few studies have investigated the value of serum tumor biomarkers in predicting VPI for NSCLC (≤3 cm).

Objective

Hence, this study aims to explore diagnostic value of CT features and serum tumor biomarkers in predicting VPI in T1-size NSCLC with a whole spectrum of histology and densities. We present this article in accordance with the STARD reporting checklist (available at https://jtd.amegroups.com/article/view/10.21037/jtd-24-294/rc).

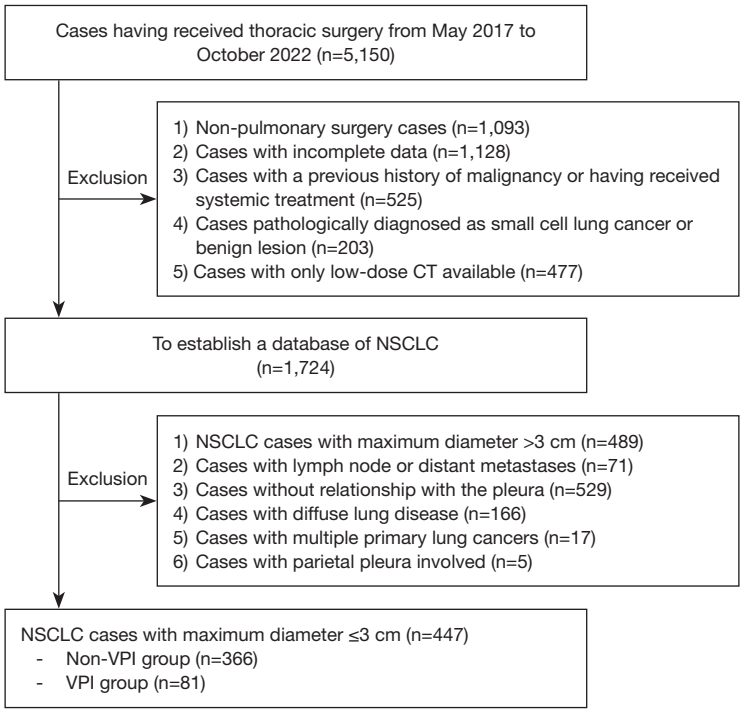

Figure 1 Flowchart of patient inclusion and exclusion. CT, computed tomography; NSCLC, non-small cell lung cancer; VPI, visceral pleura invasion.

Methods

Patient enrollment

This retrospective study was conducted in accordance with the Declaration of Helsinki (as revised in 2013). The study was approved by the institutional ethics committee of National Cancer Center/National Clinical Research Center for Cancer/Cancer Hospital & Shenzhen Hospital, Chinese Academy of Medical Sciences and Peking Union Medical College (No. KYKT2021-17-1) and individual consent for this retrospective analysis was waived. Initially, from May 2017 to October 2022, a total of 1,724 patients with NSCLC who received radical surgery were enrolled from the National Cancer Center/National Clinical Research Center for Cancer/Cancer Hospital & Shenzhen Hospital. We included those patients with (I) NSCLC confirmed by histopathology; (II) available CT images and pathological results; and (III) CT performed within 2 weeks before surgery. Exclusion criteria were as follows: (I) lesions >3 cm in long axis diameter measured on the CT image; (II) lymph node or distant metastasis confirmed by histopathology or later medical history; (III) lesions without any relationship to pleura; (IV) diffuse lung disease; (V) multiple primary lung cancers; and (VI) pathologically confirmed parietal pleura invasion. Finally, a total of 447 patients were enrolled (*Figure 1*).

CT scanning parameters

All enrolled patients received CT examinations on a 64-slice spiral CT (Optima CT660; GE Healthcare, Tokyo, Japan) or a 256-slice spiral CT (Revolution; GE Healthcare) scanner. We included 113 patients who had received only plain CT scans, and 334 patients had undergone both plain and contrast-enhanced CT scans. However, we only collected plain CT scans for further analysis in this study. The routine plain scan was performed at the end of inspiration within one breath-hold covering from the thoracic inlet to the sub-diaphragm. Scanning parameters included: voltage =120 keV, tube current =200–500 mA (automatic intelligent adjustment), slice thickness =1.25 mm, slice spacing =1.25 mm, matrix =512×512, alignment =64 mm × 0.6 mm (64-row multi-detector CT) and 256 mm × 0.6 mm (256-row multi-detector CT) and reconstruction algorithm: bone plus and asir-V 30%.

Clinical data collection

We obtained clinical data of each enrolled patient including gender, age, post-surgical pathology, visceral pleural invasion status, serum tumor biomarkers including carcino-embryonic antigen (CEA), carbohydrate antigen 12-5 (CA12-5), squamous cell carcinoma antigen (SCCA) and cytokeratin 19 fragment (CYFRA21-1), neuron-specific enolase (NSE), pro-gastrin-releasing peptide (ProGRP) from the medical record. In all cases, the post-surgical specimens were routinely processed by trained and qualified pathological technicians using elastic fiber staining, including Victoria blue staining and Verhoeff iron hematoxylin staining. The degree of pleural invasion was observed by pathologists under an ordinary light microscope and classified as follows: PL0: no visceral pleura invasion; PL1: the visceral pleura elastic layer invaded, but without exceeding the surface; PL2: visceral pleura invasion exceeding the surface; PL3: parietal pleura and chest wall invasion (19). NSCLC patients with PL1 or PL2 were assigned to the VPI group and PL0 to the non-VPI group. Patients with PL3 were excluded.

CT imaging features

The CT images were independently and blindly read by one radiologist (L.L. with 19 years of experience in chest imaging) without knowing the pathological results. Then the results were reviewed by a senior radiologist (D.L. with 37 years of experience in chest imaging) with any disagreement resolved through discussion. Imaging evaluation indices included lesion lobe location (right upper lobe, right middle lobe, right lower lobe, left upper lobe, left lower lobe), distribution (central and peripheral that are defined as lesions in the central two-third or the peripheral one-third of the lung), size (long axis diameter and short axis diameter), density type (solid, part-solid, and ground-glass opacity characterized by an attenuation increase without obscuration of underlying vasculature on lung window setting), lesion shape (oval or round and irregular), margin definition (well- and ill-defined), edge characteristics [spiculation, lobulation, pulmonary fibrous stripe, spinous process sign that is defined as nodule edges protruding sharply with the appearance of a small triangle (20)], internal characteristics [vascular convergence sign, bubble-like lucency sign that is defined as round or irregular air attenuation of 1–2 mm in diameter within a nodule (21), cavitation, calcification, and air bronchogram sign], and relationship between lesion and pleura. Vascular convergence sign was defined as the presence of at least one of these three subtypes (22), including type I, vessels passing by the lesions; type II, vessels passing through GGNs with no morphological change; and type III, distorted, dilated or tortuous vessels seen within the lesions. The relationship between the lesion and the pleura can be classified into four patterns (*Figure 2*): type I (pleural attachment): the lesion has close contact with the pleura, including type Ia: the contact length between the lesion and the pleura >1/4 of the perimeter of the lesion and type Ib: the contact length between the lesion and the pleura ≤1/4 of the perimeter of the lesion; type II (pleural indentation): the bell-shaped pleural depression between the lesion and the pleura; type III (pleural retraction): the linear shadow between the lesion and the pleura (16).

Statistical analysis

SPSS 26.0 software package (IBM Corp., Armonk, NY, USA) was used for statistical analysis. Continuous variables were described as mean ± standard deviation, and categorical variables as percentages. Shapiro-Wilk test was employed for the normality test. Student *t*-test and Mann-Whitney *U* rank-sum test were used for continuous variables with normal and non-normal distribution, respectively, and Chi-squared test was used for categorical variables. $P \leq 0.05$ was considered statistically significant. The indicators with statistically significant differences between VPI and non-VPI groups were included in the multivariate logistic regression analysis. The conditional backward method was used to determine the independent risk factors for VPI, and the forest plot was drawn according to their odds ratio (OR) values. Receiver operating characteristic (ROC) analysis was used to evaluate the diagnostic performance of logistic models based on each independent predictor and combined predictors in diagnosing VPI, with performance compared using the DeLong test (23).

Results

Clinical characteristics

A total of 447 T1-size NSCLC (≤3 cm) patients were enrolled in this study, including 429 cases of adenocarcinoma, seven cases of squamous cell carcinoma, four cases of large cell neuroendocrine carcinoma, two cases of lymphoepithelial carcinoma, two cases of carcinoid carcinoma, one case of sarcomatoid carcinoma, 1 case of combined carcinoma, and one case of adenosquamous

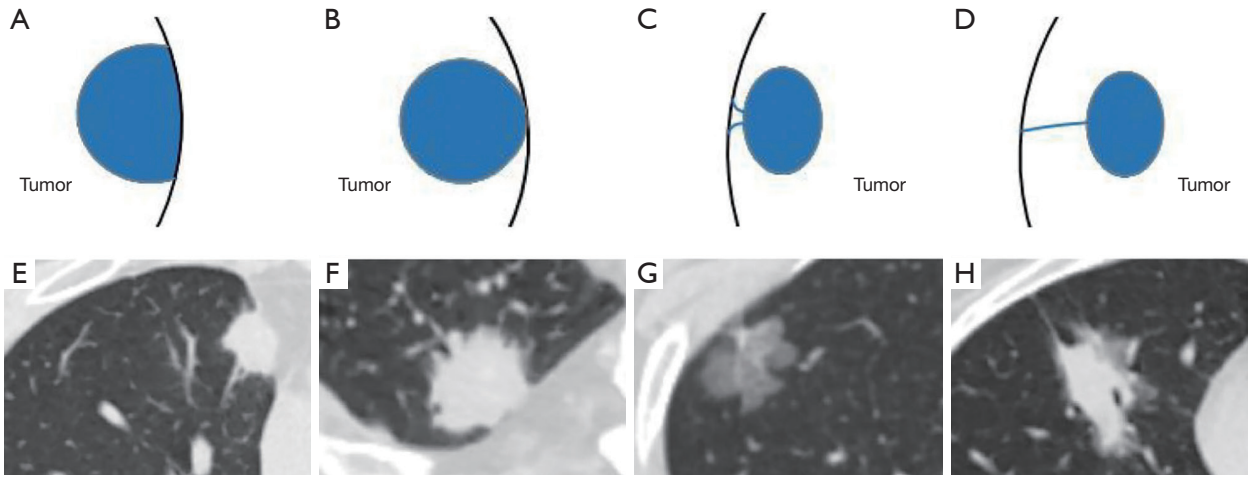

Figure 2 Definitions of lesion-pleura relationship patterns. (A) Pictogram and (E) axial CT image of a right upper lobe pleural-attached nodule with contract length >1/4 of the perimeter of the nodule (type Ia). (B) Pictogram and (F) axial CT image of a right upper lobe pleural-attached nodule with contract length ≤1/4 of the perimeter of the nodule (type Ib). (C) Pictogram and (G) axial CT image of a right upper lobe nodule with pleural indentation (type II). (D) Pictogram and (H) axial CT image of a right lower lobe nodule with linear pleural tag (type III). CT, computed tomography.

carcinoma. According to the pathological elastic fiber staining results, the patients were assigned into a VPI group (n=81) and a non-VPI group (n=366). There were 60 lesions with PL1 VPI, 21 with PL2, and no lesion with PL3. No significant difference was observed between the VPI and non-VPI groups in gender (P=0.13) and lobe location (P=0.69). The mean age of the VPI group (61.4±11.6 years) was significantly higher than that of the non-VPI group (56.4±12.6 years) (P=0.001). In addition, the VPI group had a significantly larger size both in long axis and short axis diameter than that of the non-VPI group (both P<0.001). Besides, VPI was more likely to occur for NSCLC distributed in the peripheral region (83.95%) (*Table 1*).

Tumor biomarkers

The VPI group had a significantly higher percentage of cases with abnormal CEA level, CYFRA21-1 level, and ProGRP level than that of the non-VPI group (22.22% *vs.* 7.38%, P<0.001; 35.80% *vs.* 20.22%, P=0.003; and 13.58% *vs.* 4.92%, P=0.004). For all the rest of the tumor biomarkers, no significant differences were observed between the VPI group and the non-VPI group (NSE, P=0.64; SCCA, P=0.90; CA12-5, P=0.91) (*Table 2*).

CT morphological features

Regarding lesion density, over 4/5 (80.25%) were solid lesions in the VPI group (*Figure 3A-3D*), followed by part-solid lesions (19.75%) (*Figure 3E-3H*). In contrast, most of the lesions were sub-solid lesions (34.7% for part-solid lesions + 43.17% for ground-glass lesions) in the non-VPI group, and the distribution of lesion density between these two groups was significantly different (P<0.001). In particular, VPI was present in none of these 158 NSCLC cases with ground-glass lesions. Regarding lesion-pleura relationship patterns, the incidence of type Ia was predominant in the VPI group (43/81, 53.09%), while these four types were more evenly distributed in the non-VPI group. Specifically, VPI was present in 31.85% (43/135) of type Ia cases, 10.74% (13/121) of type Ib cases, 19.82% (22/111) of type II cases and 3.75% (3/80) of type III cases, respectively (*Table 3* and *Figure 4*). In addition, a significantly higher percentage of spiculation (91.36% *vs.* 73.77%, P=0.001), pulmonary fibrous stripe (56.79% *vs.* 27.60%, P<0.001), spinous process sign (11.11% *vs.* 3.83%, P=0.007), cavitation (6.17% *vs.* 1.37%, P=0.008), and calcification (7.41% *vs.* 1.64%, P=0.004) were present in the VPI group compared with the non-VPI group. However, no significant difference was observed in shape (P=0.14),

Table 1 Clinical characteristics between VPI group and non-VPI group

Clinical characteristics	Total patients (n=447)	VPI group (n=81)	Non-VPI group (n=366)	P value
Gender				0.13
Male	182 (40.72)	39 (48.15)	143 (39.07)	
Female	265 (59.28)	42 (51.85)	223 (60.93)	
Age (years)	58.9±12.1	61.4±11.6	56.4±12.6	0.001*
Size (cm)				
Long axis diameter	1.8±0.7	2.1±0.7	1.6±0.7	<0.001*
Short axis diameter	1.4±0.6	1.6±0.6	1.2±0.6	<0.001*
Lobe location				0.69
Right lung				
Superior lobe	126	20 (24.69)	106 (28.96)	
Middle lobe	59	14 (17.28)	45 (12.3)	
Inferior lobe	90	16 (19.75)	74 (20.22)	
Left lung				
Superior lobe	90	16 (19.75)	83 (22.68)	
Inferior lobe	73	15 (18.52)	58 (15.85)	
Distribution				0.01*
Central	39	13 (16.05)	26 (7.1)	
Peripheral	408	68 (83.95)	340 (92.9)	

Data are presented as n (%), mean ± SD, or n. *, statistically significant. VPI, visceral pleura invasion; SD, standard deviation.

margin definition (P=0.12), lobulation (P=0.59), bubble-like lucency (P=0.10), air bronchogram sign (P=0.32), and vascular convergence sign (P=0.28) of NSCLC lesions between the VPI group and the non-VPI group (*Table 3*).

Multivariate logistic regression analysis identified the lesion-pleura relationship patterns including type Ia [OR =20.689; 95% confidence interval (CI): 5.058–84.622; P<0.001], type Ib (OR =5.155; 95% CI: 1.178–22.552; P=0.03), type II (OR =7.154; 95% CI: 1.733–29.53; P=0.007) with type III as reference, solid lesion density (OR =9.954; 95% CI: 4.976–19.911; P<0.001) with sub-solid as reference as the independent predictors for VPI (*Table 4* and *Figure 5A*). In predicting VPI, the combined model was built by combining all the independent risk factors, yielding an area under the ROC curve (AUC) of 0.885 (95% CI: 0.852–0.913). The combined model significantly outperformed models based on the single independent risk factor, including lesion density (AUC =0.833; 95% CI: 0.795–0.867; P<0.001), lesion-pleura relationship patterns (AUC =0.655; 95% CI: 0.609–0.699; P<0.001) (*Figure 5B*).

Discussion

Key findings, comparison with similar researches and explanations of findings

This study explored diagnostic value of preoperative staging CT imaging features and serum tumor biomarker levels in predicting VPI in T1-size NSCLC with a spectrum of histology and densities. The result showed that the solid lesion density and lesion-pleura relationship patterns (pleural attachment and indentation), but no serum biomarkers are the independent predictors for VPI in patients with NSCLC (≤3 cm).

Among all the CT predictors for VPI in T1-sized NSCLC, lesion density type was the most important predictor with the highest OR (solid:sub-solid =9.954:1) and best diagnostic performance among all the models based on the single CT predictor. Our study found that VPI was more common in solid nodules (65/146, 44.5%), compared with part-solid (16/143, 11.2%) and GGNs (0/158, 0%). In particular, none of the ground-glass T1-size NSCLC lesions

Table 2 Analysis of lung cancer tumor biomarkers in the VPI and non-VPI groups

Tumor biomarkers	Total (n=447)	VPI group (n=81)	Non-VPI group (n=366)	P value
CEA (ng/mL)				<0.001*
<5	402 (89.93)	63 (77.78)	339 (92.62)	
≥5	45 (10.07)	18 (22.22)	27 (7.38)	
CYFRA21-1 (ng/mL)				0.003*
<3.3	344 (76.96)	52 (64.20)	292 (79.78)	
≥3.3	103 (23.04)	29 (35.80)	74 (20.22)	
NSE (ng/mL)				0.64
<16.3	419 (93.74)	75 (92.59)	344 (93.99)	
≥16.3	28 (6.26)	6 (7.41)	22 (6.01)	
SCCA (ng/mL)				0.90
<2.7	435 (97.32)	79 (97.53)	356 (97.27)	
≥2.7	12 (2.68)	2 (2.47)	10 (2.73)	
ProGRP (pg/mL)				0.004*
<69.2	418 (93.51)	70 (86.42)	348 (95.08)	
≥69.2	29 (6.49)	11 (13.58)	18 (4.92)	
CA12-5 (U/mL)				0.91
<35	442 (98.89)	80 (98.77)	362 (98.91)	
≥35	5 (1.12)	1 (1.23)	4 (1.09)	

Data are presented as n (%). *, statistically significant. VPI, visceral pleura invasion; CEA, carcino-embryonic antigen; CYFRA21-1, cytokeratin 19 fragment; NSE, neuron-specific enolase; SCCA, squamous cell carcinoma antigen; ProGRP, pro-gastrin-releasing peptide; CA12-5, carbohydrate antigen 12-5.

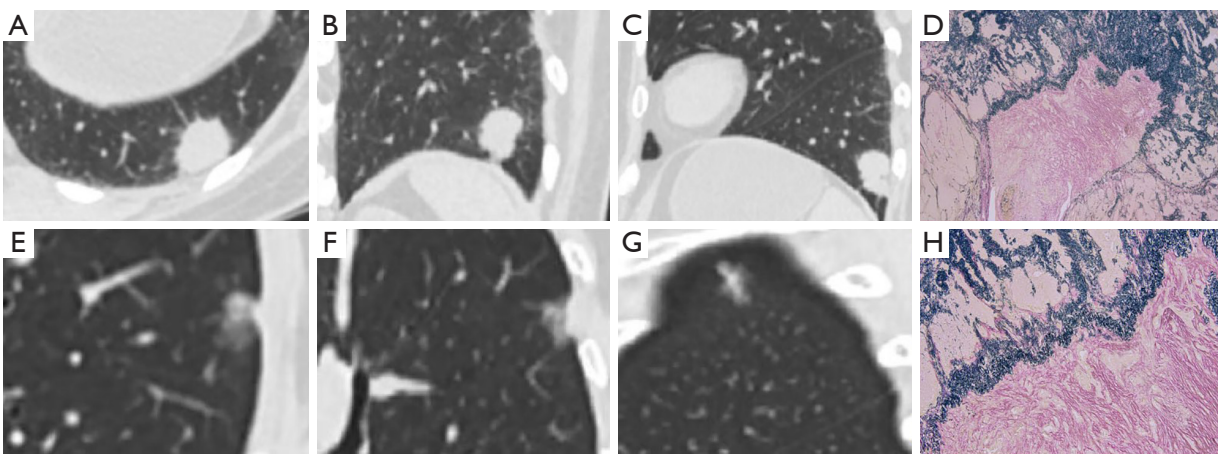

Figure 3 Two representative cases of solid and subsolid lesions with positive VPI. (A-D) CT images of a 53-year-old female with histologically confirmed invasive adenocarcinoma at three different views show a subpleural solid nodule located in the lower lobe of the left lung. The lesion has a well-defined margin and multiple tiny spiculations. The relationship between the lesion and the adjacent interlobar pleura was type Ia (pleural attachment >1/4). Elastic staining confirmed PL2 VPI (100×). (E-H) CT images of a 66-year-old female with histologically confirmed invasive adenocarcinoma at different views show a subpleural part-solid nodule located in the upper lobe of the left lung with a type II pattern (pleural indentation). Elastic staining confirmed PL1 VPI (100×). PL1: the visceral pleura elastic layer invaded, but without exceeding the surface; PL2: visceral pleura invasion exceeding the surface. VPI, visceral pleura invasion; CT, computed tomography.

Table 3 CT morphological analysis of VPI group and non-VPI group

CT characteristics	Total (n=447)	VPI group (n=81)	Non-VPI group (n=366)	P value
Density				<0.001*
Solid	146	65 (80.25)	81 (22.13)	
Part-solid	143	16 (19.75)	127 (34.70)	
GGN	158	0 (0.00)	158 (43.17)	
Shape				0.14
Oval or round	366	71 (87.65)	295 (80.60)	
Irregular	81	10 (12.35)	71 (19.40)	
Margin definition				0.12
Well-defined	427	80 (98.77)	347 (94.81)	
Ill-defined	20	1 (1.23)	19 (5.19)	
Lobulation				0.59
Absence	28	4 (4.94)	24 (6.56)	
Presence	419	77 (95.06)	342 (93.44)	
Spiculation				0.001*
Absence	103	7 (8.64)	96 (26.23)	
Presence	344	74 (91.36)	270 (73.77)	
Spinous process sign				0.007*
Absence	424	72 (88.89)	352 (96.17)	
Presence	23	9 (11.11)	14 (3.83)	
Pulmonary fibrous stripe				<0.001*
Absence	300	35 (43.21)	265 (72.40)	
Presence	147	46 (56.79)	101 (27.60)	
Bubble-like lucency				0.10
Absence	396	76 (93.83)	320 (87.43)	
Presence	51	5 (6.17)	46 (12.57)	
Cavitation				0.008*
Absence	437	76 (93.83)	361 (98.63)	
Presence	10	5 (6.17)	5 (1.37)	
Calcification				0.004*
Absence	435	75 (92.59)	360 (98.36)	
Presence	12	6 (7.41)	6 (1.64)	
Air bronchogram sign				0.32
Absence	282	55 (67.90)	227 (62.02)	
Presence	165	26 (32.10)	139 (37.98)	
Vascular convergence sign				0.28
Absence	46	11 (13.58)	35 (9.56)	
Presence	401	70 (86.42)	331 (90.44)	

Table 3 *(continued)*

Table 3 *(continued)*

CT characteristics	Total (n=447)	VPI group (n=81)	Non-VPI group (n=366)	P value
Lesion-pleura relationship patterns				<0.001*
Type Ia (pleural attachment >1/4)	135	43 (53.09)	92 (25.14)	
Type Ib (pleural attachment ≤1/4)	121	13 (16.05)	108 (29.51)	
Type II (pleural indentation)	111	22 (27.16)	89 (24.32)	
Type III (linear pleural retraction)	80	3 (3.70)	77 (21.04)	

Data are presented as n or n (%). *, statistically significant. VPI, visceral pleura invasion; CT, computed tomography; GGN, ground-glass nodule.

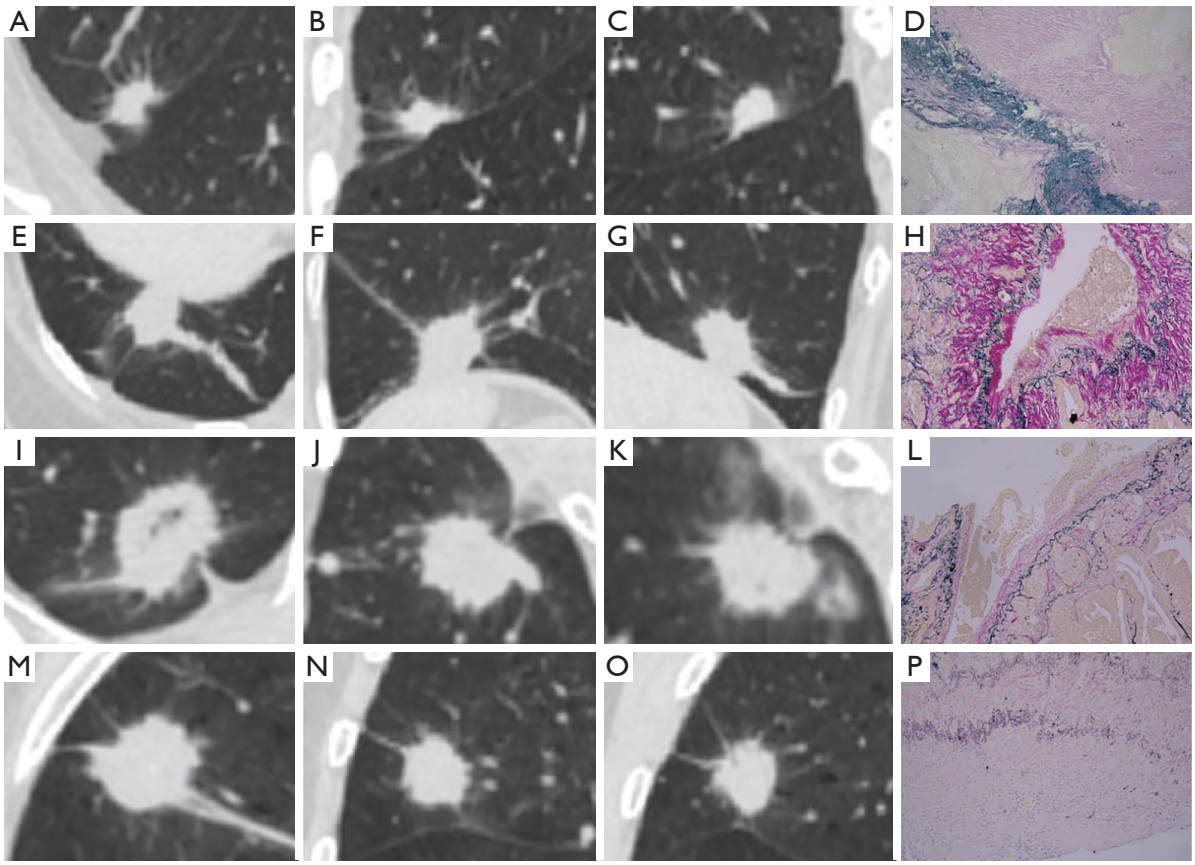

Figure 4 Four representative positive VPI lesions with four lesion-pleura relationship patterns. (A-D) CT images of a 65-year-old male with histologically confirmed invasive adenocarcinoma at three different views (A-C) show a subpleural solid nodule located in the upper lobe of the right lung with type Ia (pleural attachment >1/4) lesion-pleura attachment pattern. Elastic staining confirmed PL2 VPI (D; 100×). (E-H) CT images of a 53-year-old female with histologically confirmed invasive adenocarcinoma at different views (E-G) show a subpleural solid nodule located in the lower lobe of the right lung with a type Ib pattern (pleural attachment ≤1/4). Elastic staining confirmed PL2 VPI (H; 100×). (I-L) CT images of a 58-year-old male with histologically confirmed invasive adenocarcinoma at different views (I-K) show a subpleural solid nodule located in the upper lobe of the left lung with a type II pattern (pleural indentation). Elastic staining confirmed PL2 VPI (L; 100×). (M-P) CT images of a 65-year-old male with histologically confirmed invasive adenocarcinoma at different views (M-O) show a subpleural solid nodule located in the upper lobe of the right lung with a type III pattern (multiple linear pleural retractions). Elastic staining confirmed PL1 VPI (P; 100×). PL1: the visceral pleura elastic layer invaded, but without exceeding the surface; PL2: visceral pleura invasion exceeding the surface. VPI, visceral pleura invasion; CT, computed tomography.

Table 4 Multivariate logistic regression analysis in predicting VPI

Characteristics	Adjusted OR (95% CI)	P value
CEA	0.749 (0.304, 1.847)	0.53
CYFRA21-1	1.048 (0.491, 2.234)	0.90
ProGRP	0.419 (0.141, 1.248)	0.12
Distribution	0.962 (0.34, 2.723)	0.94
Long axis diameter	1.262 (0.437, 3.64)	0.67
Short axis diameter	1.894 (0.548, 6.551)	0.31
Cavitation	1.236 (0.246, 6.22)	0.80
Calcification	0.557 (0.116, 2.676)	0.47
Spiculation	0.496 (0.18, 1.368)	0.18
Spinous process sign	1.065 (0.334, 3.394	0.92
Pulmonary fibrous stripe	0.725 (0.337, 1.56)	0.41
Age	1.002 (0.974, 1.03)	0.89
Lesion-pleura relationship patterns		
Type Ia (pleural attachment >1/4)	20.689 (5.058, 84.622)	<0.001*
Type Ib (pleural attachment ≤1/4)	5.155 (1.178, 22.552)	0.03*
Type II (pleural indentation)	7.154 (1.733, 29.53)	0.007*
Type III (pleural retraction)	Reference	
Density type		
Solid	9.954 (4.976, 19.911)	<0.001*
Sub-solid	Reference	

*, statistically significant. VPI, visceral pleura invasion; OR, odds ratio; CI, confidence interval; CEA, carcino-embryonic antigen; CYFRA21-1, cytokeratin 19 fragment; ProGRP, pro-gastrin-releasing peptide.

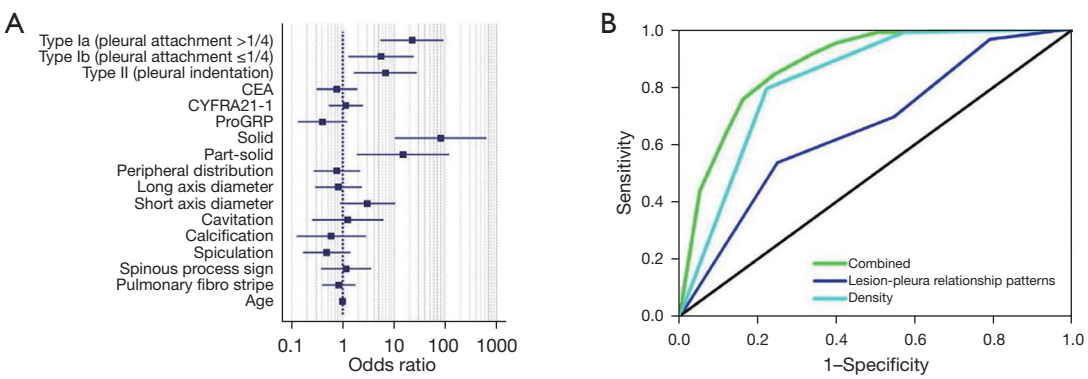

Figure 5 The forest plot (A) of multivariate analysis and ROC curve of three models (B). CEA, carcino-embryonic antigen; CYFRA21-1, cytokeratin 19 fragment; ProGRP, pro-gastrin-releasing peptide; ROC, receiver operating characteristic.

(0/158) was proven to be with VPI, suggesting that ground-glass opacity is a reliable negative predictor of the VPI, which is consistent with most previous studies that none of the pure ground-glass lesion had VPI (8,12,18). However, another study by Zhao *et al.* reported an incidence of VPI as high as 17.4% (12/69) in pure ground-glass NSCLC (≤3 cm) (17). This discrepancy might be attributed to the inconsistent subjective evaluation criteria and inter-observer variability, which needs further confirmation with a larger sample in the future. In addition, a study showed that the solid proportion of the lesion is positively associated with the risk of VPI (8), suggesting density is the first important feature that should be considered when evaluating VPI. With automatic segmentation tools available using artificial intelligence (AI), the volumetrical CT values might be more appropriate to characterize the nodule instead of arbitrarily classifying nodule into solid, part-solid, and GGN, which needs further confirmation.

In this study, the relationship patterns between tumor and pleura were classified into four types, among which type Ia (pleural attachment >1/4) had the highest OR, followed by type II (pleural indentation) and type Ib (pleural attachment ≤1/4) to predict VPI in T1-sized NSCLC. Several previous studies showed that the contact surface area (12) or length (9,15) between tumor and pleura is highly predictive of VPI in T1-size NSCLC, which is consistent with the result of our study. Interestingly, the type II (pleural indentation) lesion-pleura relationship pattern that showed no direct contact between lesion and pleura was more frequently present in the VPI group than the type Ib (pleural attachment ≤1/4) pattern. Consistently, previous studies showed that a non-linear pleural tag sign equivalent to our type II pattern (pleural indentation) in our study was significantly associated with VPI (9,13,14). Histopathology studies (24,25) showed that pleural tags might be caused by local edema, tumor invasion, inflammation, fibrosis, etc., which explains the high sensitivity but low specificity of using pleural tags to predict VPI for T1-size NSCLC. Besides, unlike the study by Yang *et al.* (15), our study showed that serum tumor biomarkers were unreliable for predicting VPI in T1-size NSCLC.

Besides, in our study, we designed quite strict inclusion and exclusion criteria. For instance, we only enrolled T1-sized NSCLC patients without lymph node metastasis or without parietal pleural invasion. The reason we excluded T1-sized NSCLC patients with lymph node metastasis or with parietal pleural invasion is that we intended to focus on staged IA and staged IB NSCLC. T1-sized NSCLC with parietal pleural invasion will be staged as T3. Also, if we included N1-N3, the clinical stage could vary from IA (T1N0) to IIIB (T1N3), leading to different surgical approaches or treatment decisions. Therefore, we excluded these staging factors that could affect the treatment decisions (e.g., T stage, N stage).

Limitations and implications and actions needed

This is a retrospective study performed in a single institution with a relatively small number of lesions with positive VPI. To reduce the possibility of selection bias, we need more studies with larger sample sizes to confirm our results. In addition, in this study, we did not measure the contact surface or length between lesion and pleura for the pleura-attachment pattern because we believe that it is a simple sign and more operable in the clinical setting to dichotomize lesion-pleura attachment patterns into type Ia and type Ib based on the contact length. In addition, we did not perform a strict double-blind reading but a revision of a previous reading by a senior radiologist to mimic the real practice. Lastly, with the emergence of AI-powered automatic segmentation tools, more quantitative morphological measurements should be investigated in the future.

Conclusions

The combination of solid lesion density, pleural attachment, and pleural indentation can improve the accuracy of predicting VPI in T1-sized NSCLC with a diameter ≤3 cm. However, serum tumor markers showed limited predictive power.

Acknowledgments

Funding: This work was supported by the Shenzhen Science and Technology Program (No. KCXFZ20201221173008022), the National Cancer Center/National Clinical Research Center for Cancer/Cancer Hospital & Shenzhen Hospital, Chinese Academy of Medical Sciences and Peking Union Medical College, Shenzhen (No. SZ2020QN001), the Shenzhen Clinical Research Center for Cancer (No. [2021] 287), and the Shenzhen High-Level Hospital Construction Fund.

Footnote

Reporting Checklist: The authors have completed the STARD reporting checklist. Available at https://jtd.amegroups.com/

article/view/10.21037/jtd-24-294/rc

Data Sharing Statement: Available at https://jtd.amegroups.com/article/view/10.21037/jtd-24-294/dss

Peer Review File: Available at https://jtd.amegroups.com/article/view/10.21037/jtd-24-294/prf

Conflicts of Interest: All authors have completed the ICMJE uniform disclosure form (available at https://jtd.amegroups.com/article/view/10.21037/jtd-24-294/coif). All authors report that this study was supported by the Shenzhen Science and Technology Program (No. KCXFZ20201221173008022), the National Cancer Center/National Clinical Research Center for Cancer/Cancer Hospital & Shenzhen Hospital, Chinese Academy of Medical Sciences and Peking Union Medical College, Shenzhen (No. SZ2020QN001), the Shenzhen Clinical Research Center for Cancer (No. [2021] 287), and the Shenzhen High-Level Hospital Construction Fund. The authors have no other conflicts of interest to declare.

Ethical Statement: The authors are accountable for all aspects of the work in ensuring that questions related to the accuracy or integrity of any part of the work are appropriately investigated and resolved. This retrospective study was conducted in accordance with the Declaration of Helsinki (as revised in 2013). The study was approved by the institutional ethics committee of National Cancer Center/National Clinical Research Center for Cancer/Cancer Hospital & Shenzhen Hospital, Chinese Academy of Medical Sciences and Peking Union Medical College (No. KYKT2021-17-1), and individual consent for this retrospective analysis was waived.

References

1. Sung H, Ferlay J, Siegel RL, et al. Global Cancer Statistics 2020: GLOBOCAN Estimates of Incidence and Mortality Worldwide for 36 Cancers in 185 Countries. CA Cancer J Clin 2021;71:209-49.
2. Huang W, Deng HY, Lin MY, et al. Treatment Modality for Stage IB Peripheral Non-Small Cell Lung Cancer With Visceral Pleural Invasion and ≤3 cm in Size. Front Oncol 2022;12:830470.
3. Pathak R, Goldberg SB, Canavan M, et al. Association of Survival With Adjuvant Chemotherapy Among Patients With Early-Stage Non-Small Cell Lung Cancer With vs Without High-Risk Clinicopathologic Features. JAMA Oncol 2020;6:1741-50.
4. Asamura H. PL04.03: 9th Edition TNM Staging Classification: Lung Cancer. WCLC. 2023. Available online: https://rs.yiigle.com/cmaid/1495697
5. Yu Y, Huang R, Wang P, et al. Sublobectomy versus lobectomy for long-term survival outcomes of early-stage non-small cell lung cancer with a tumor size ≤2 cm accompanied by visceral pleural invasion: a SEER population-based study. J Thorac Dis 2020;12:592-604.
6. Mathey-Andrews C, Abruzzo AR, Venkateswaran S, et al. Segmentectomy vs Lobectomy for Early Non-Small Cell Lung Cancer With Visceral Pleural Invasion. Ann Thorac Surg 2024;117:1007-14.
7. Choi SY, Moon MH, Moon Y. The prognosis of small-sized non-small cell lung cancer with visceral pleural invasion after sublobar resection. Transl Cancer Res 2020;9:6431-43.
8. Ahn SY, Park CM, Jeon YK, et al. Predictive CT Features of Visceral Pleural Invasion by T1-Sized Peripheral Pulmonary Adenocarcinomas Manifesting as Subsolid Nodules. AJR Am J Roentgenol 2017;209:561-6.
9. Shi J, Li F, Yang F, et al. The combination of computed tomography features and circulating tumor cells increases the surgical prediction of visceral pleural invasion in clinical T1N0M0 lung adenocarcinoma. Transl Lung Cancer Res 2021;10:4266-80.
10. Yang S, Yang L, Teng L, et al. Visceral pleural invasion by pulmonary adenocarcinoma ≤3 cm: the pathological correlation with pleural signs on computed tomography. J Thorac Dis 2018;10:3992-9.
11. Deng HY, Li G, Luo J, et al. Novel biologic factors correlated to visceral pleural invasion in early-stage non-small cell lung cancer less than 3 cm. J Thorac Dis 2018;10:2357-64.
12. Sun Q, Li P, Zhang J, et al. CT Predictors of Visceral Pleural Invasion in Patients with Non-Small Cell Lung Cancers 30 mm or Smaller. Radiology 2024;310:e231611.

13. Onoda H, Higashi M, Murakami T, et al. Correlation between pleural tags on CT and visceral pleural invasion of peripheral lung cancer that does not appear touching the pleural surface. Eur Radiol 2021;31:9022-9.
14. Hsu JS, Han IT, Tsai TH, et al. Pleural Tags on CT Scans to Predict Visceral Pleural Invasion of Non-Small Cell Lung Cancer That Does Not Abut the Pleura. Radiology 2016;279:590-6.
15. Yang Y, Xie Z, Hu H, et al. Using CT imaging features to predict visceral pleural invasion of non-small-cell lung cancer. Clin Radiol 2023;78:e909-17.
16. Kim H, Goo JM, Kim YT, et al. CT-defined Visceral Pleural Invasion in T1 Lung Adenocarcinoma: Lack of Relationship to Disease-Free Survival. Radiology 2019;292:741-9.
17. Zhao LL, Xie HK, Zhang LP, et al. Visceral pleural invasion in lung adenocarcinoma ≤3 cm with ground-glass opacity: a clinical, pathological and radiological study. J Thorac Dis 2016;8:1788-97.
18. Zhao Q, Wang JW, Yang L, et al. CT diagnosis of pleural and stromal invasion in malignant subpleural pure ground-glass nodules: an exploratory study. Eur Radiol 2019;29:279-86.
19. Goldstraw P. New staging system: how does it affect our practice? J Clin Oncol 2013;31:984-91.
20. Shi Z, Wang Y, He X. Differential diagnosis of solitary pulmonary nodules with dual-source spiral computed tomography. Exp Ther Med 2016;12:1750-4.
21. Fan L, Liu SY, Li QC, et al. Pulmonary malignant focal ground-glass opacity nodules and solid nodules of 3cm or less: comparison of multi-detector CT features. J Med Imaging Radiat Oncol 2011;55:279-85.
22. Gao F, Li M, Ge X, et al. Multi-detector spiral CT study of the relationships between pulmonary ground-glass nodules and blood vessels. Eur Radiol 2013;23:3271-7.
23. DeLong ER, DeLong DM, Clarke-Pearson DL. Comparing the areas under two or more correlated receiver operating characteristic curves: a nonparametric approach. Biometrics 1988;44:837-45.
24. Meng Y, Gao J, Wu C, et al. The prognosis of different types of pleural tags based on radiologic-pathologic comparison. BMC Cancer 2022;22:919.
25. Han J, Xiang H, Ridley WE, et al. Pleural tail sign: pleural tags. J Med Imaging Radiat Oncol 2018;62 Suppl 1:37.

Cite this article as: Li L, Yang Q, Luo D, Wang X, Liu Z, Huang R. Baseline computed tomography imaging findings could assist in early diagnosis of visceral pleural invasion for newly discovered early subpleural non-small cell lung cancer: T1 or T2. J Thorac Dis 2024;16(9):5779-5791. doi: 10.21037/jtd-24-294